

FORBIDDEN LINE PROFILES FROM MASSIVE BINARY COLLIDING WINDS

RYAN BESSEY

Department of Physics & Astronomy, Berry College, Mount Berry, GA, 30149-0159

RICHARD IGNACE

Department of Physics, Astronomy & Geology, East Tennessee State University, Johnson City, TN 37164

ABSTRACT

We investigate the effects on the emission profile of a Wolf-Rayet (WR) wind colliding with an O star wind. Since the mass loss rate of the WR star far exceeds that of the O star, the O star effectively forms a cavity in the WR wind. The cavity takes on a spiral shape as the O star orbits the WR. This cavity produces interesting observable effects in the emission profiles of forbidden lines. We model the effects of a spiral cavity on the emission profile for both circular and elliptical binary orbits. The presence of a cavity leads to a deficit in the otherwise flat-top profile. The opening angle of the cavity, viewing inclination of the binary, and eccentricity of the orbit govern the profile shape.

Subject headings: stars – winds, outflows – Wolf Rayet

1. INTRODUCTION

In 1867, Wolf and Rayet discovered a type of star that has spectral lines similar to novae. The similarity led astronomers to believe that there is a continuous outflow of mass from WR stars. They estimated that the star was losing mass at a rate of 10^{-5} solar masses per year, and the terminal velocity of the outflow was about 1000 km/s (Cassinelli & Lamers 1999). The emission of particles from a star is called a stellar wind.

In this paper, we study the forbidden lines that are produced by the spontaneous decay of electrons from metastable states to lower energy states in WR winds. We can assume that the lines are optically thin and, since the lines form over large radius we shall ignore stellar occultation.

The forbidden lines that form in stellar winds experience line broadening owing to the wind flow. We can assume the wind has reached its terminal velocity. For simplicity, we also assume that the wind velocity in this model is spherically symmetric, though in general this may not be true. A region in the wind where the observed Doppler-shifted velocities are the same is referred to as an "isovelocity zone." If θ is the polar angle between the observer axis and the velocity vector, then the isovelocity zones are determined by $w_z = v_z/v_\infty$, or $w_z = -v(r)/v_\infty \cos(\theta)$, where z refers to the observer axis, v_z is the projected velocity shift owing to the Doppler effect, $v(r)$ is the radial wind velocity profile, and v_∞ is the wind terminal speed. The parameter w_z is then a normalized velocity shift of a point in the wind with respect to the observer. In this model, $w_z = -1$ refers to the most blue-shifted and $w_z = +1$ refers to the most red-shifted. For constant spherical expansion, the isovelocity zones become cones of constant θ centered on the observer axis.

The flux of emission for an optically thin line is given by the following volume integral (Mihalas 1978):

$$F = \frac{1}{D^2} \int j(r) dV, \quad (1)$$

where $j(r)$ is the emissivity, and D is the distance from Earth to the source, and we assume the emissivity is a function of radius only. In this case, the emission profile will always be

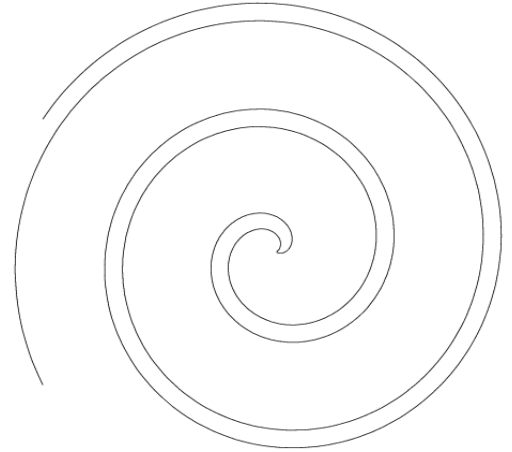


FIG. 1.— Geometry of a spiral cavity

flat-top in appearance. This means that the total flux from every isovelocity zone is the same.

We define the critical radius at the distance in the wind where the electron density equals the critical density. At this radius, the emissivity changes from a linear function of density to a quadratic function of density, thus affecting the total emission (Ignace & Brimeyer 2006). Inside this radius, the forbidden lines form from collisions and outside the critical radius, the forbidden lines form from radiative decay. It turns out that the total flux emitted inside the critical radius equals the total flux emitted outside the critical radius.

Some WR stars are known to be in binaries. In our model, we consider a WR star and O star companion. Because the momentum of the outflow from the Wolf-Rayet greatly exceeds that of the O star, the companion acts as an obstacle within the outflow of mass from the Wolf-Rayet. In effect, this obstacle produces a cavity in the wind. Then, as the stars orbit each other, the cavity takes on a spiral shape. An example spiral is shown in Figure 1. To visualize the spiral, imagine

spinning around while holding a water hose. The water moves radially outward at all times, but the source of the water, the hose, is rotating and so the perceived pattern is a spiral. The analog to the O star is the hose, and the analog to the spiral cavity is the shape of the flow of water after leaving the hose.

The absence of emitting matter due to the cavity creates a deviation from a flat-top profile. We will assume that the O star wind does not contribute to the line emission. Also, in these models we ignore the emission from the shock layer, formed by the wind collision. The shock layer may in fact contribute significantly to the profile by adding emission.

The parameters that affect the shape of the emission line are the opening angle of the cavity, the viewing inclination, the ratio of the binary separation to the critical radius, and, in the case of an elliptical orbit, the eccentricity.

The opening angle of the cavity is determined by the relative mass loss rates of each of the stars. Let $Q = \dot{M}_{\text{WR}} v_{\text{WR}} / \dot{M}_{\text{O}} v_{\text{O}}$, then the opening angle β is determined by

$$\tan(\beta) - \beta = \pi \left(\frac{Q}{1-Q} \right). \quad (2)$$

Here, β is the half-opening angle, \dot{M} is the mass loss rate, and v is the terminal speed (Canto, Raga, & Wilkin 1996). Since v_{WR} and v_{O} are generally known, and β can be determined from the emission profile, then it should be possible to determine $\dot{M}_{\text{WR}} / \dot{M}_{\text{O}}$. Analysis of this equation reveals that a larger ratio of Wolf-Rayet mass loss rate to O star mass loss rate means a *smaller* cavity opening angle. If we can determine the mass loss rate of the Wolf-Rayet through observations, then, by knowing β we can determine the mass loss rate of the O star. Also, if we can use known measurements of mass loss rates for both stars, then we can determine β from the formula. This can serve as a useful check of the model.

2. RESULTS

Before investigating the spiral cavity, it is helpful to consider a model for a simple linear cavity. Imagine that the WR and O stars are stationary, with no orbital motion. The cavity becomes a cone of constant angle and fixed phase relative to the observer. Plots of the emission profile with the linear cavity when the system is viewed edge-on are shown in Figure 2. The half-opening angle in each of these profiles is 30° . From top left, the positions of the linear cavity are $\theta = 0^\circ, 30^\circ, 45^\circ, 60^\circ, 90^\circ, 120^\circ, 135^\circ, 150^\circ, 180^\circ$. Except for the case where the cavity is orthogonal to the line of sight ($\theta = 90^\circ$), in general the emission profiles are asymmetric about line center. In the case that the cavity is centered on the line of sight, ($\theta = 0^\circ, 180^\circ$), no emission is observed for the isovelocity zones between 0° and β or between $(180^\circ - \beta)$ and 180° .

For a fully developed spiral cavity, emission profiles for various β values are summarized in Figure 3. The four boxes are different viewing inclinations, $i = 0^\circ, 30^\circ, 60^\circ, 90^\circ$. In each box, $\beta = 30^\circ, 50^\circ, 70^\circ$. Also apparent is that different viewing inclinations change the shape of the profile in interesting ways. Notice that all of these profiles are symmetric about line center, which is always the case when the orbit is circular. Looking at the case when $i = 90^\circ$ which is when the system is viewed edge-on, we notice that the extremes in the profile are affected most by the cavity. The opposite is true when $i = 0^\circ$ which is when the system is viewed pole-on. In this case the extremes of the profile are flat-top, meaning they are not affected by the cavity at all. This is expected because the

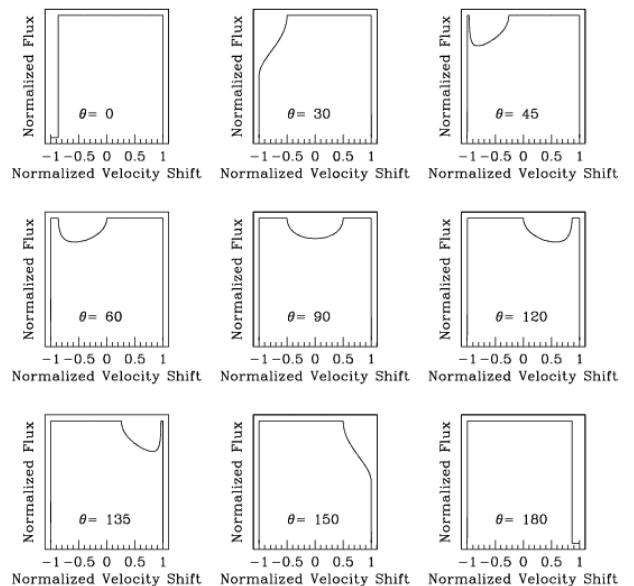


FIG. 2.— Emission profile of linear cavity at different positions.

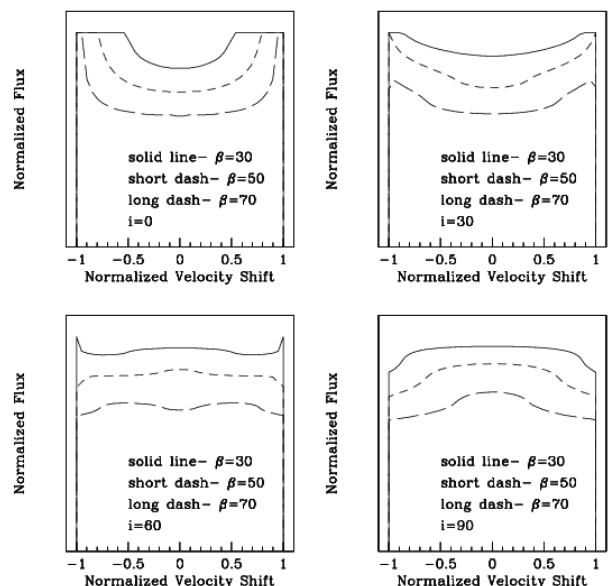


FIG. 3.— Emission profile of spiral cavity with varied opening angle and inclination.

cavity never penetrates these isovelocity zones. In fact, notice that the emission profile when $i = 0^\circ$ in Figure 3 is qualitatively the same as when $\theta = 90^\circ$ in Figure 2. This is always the case when $i = 0^\circ$, because the cavity is always in the same isovelocity zones.

Another important parameter is the ratio of binary (r_0) separation to critical radius (r_c). When the binary separation is much less than the critical radius, the cavity will have a large effect on the line profile. When the binary separation is at or near the critical radius, the cavity will affect the profile a little less because the cavity is only in the outer portion of the wind. In the limit that the binary separation is much greater than the critical radius, the cavity will have little or no effect. Behavior of the line shapes for these different cases are shown in Figure

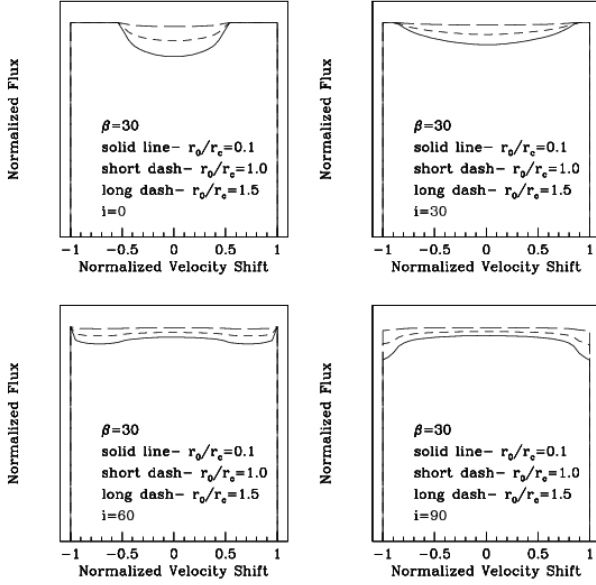


FIG. 4.— Emission profile of spiral cavity with varied binary separation and inclination.

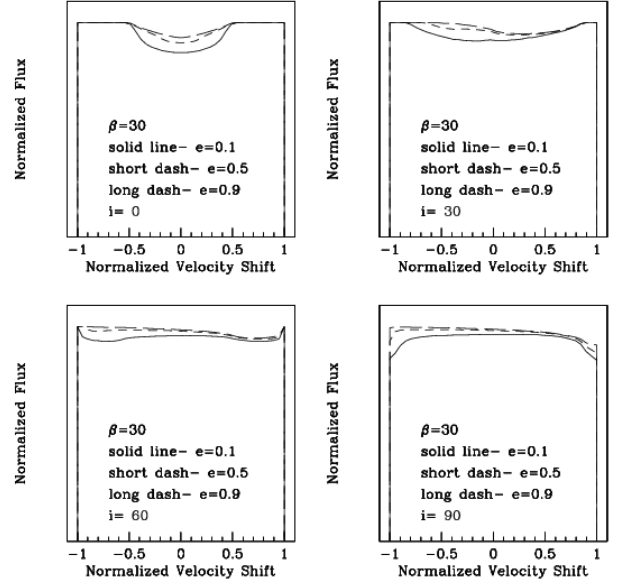


FIG. 6.— Emission profile of spiral cavity with varied eccentricity and inclination.

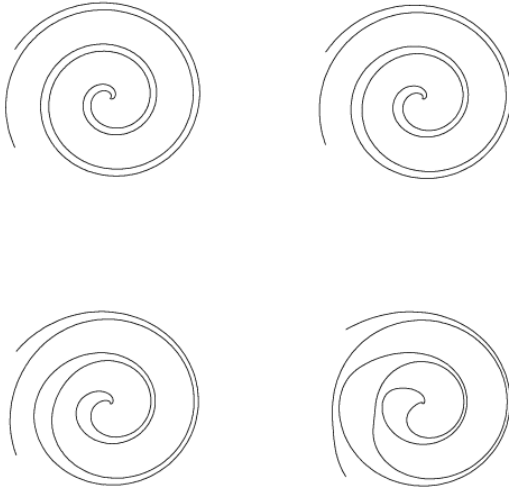


FIG. 5.— Geometry of elliptical spirals; top left $e = 0.1$; top right: $e = 0.3$; bottom left: $e = 0.5$; bottom right: $e = 0.7$.

4. The viewing inclination is again $i = 0^\circ, 30^\circ, 60^\circ, 90^\circ$, and $\beta = 30^\circ$ for all four panels, but $r_0/r_c = 0.1, 1.0, 1.5$. Notice that as r_0/r_c increases, the profile approaches flat-top.

The geometry of the cavity at various eccentricities is shown in Figure 5. The plots in Figure 6 are of the emission profile for various eccentricities. Again, $i = 0^\circ, 30^\circ, 60^\circ, 90^\circ$, but now $e = 0.1, 0.5, 0.9$. As the eccentricity increases, the profile becomes more and more asymmetric. In these plots the viewer is looking along the major axis. The point in the orbit closest to the viewer is periastron. The point in the orbit furthest from the viewer is apastron. Notice how higher eccentricity means a greater deficit at apastron than at periastron. The reason for this is Kepler's Second Law, which tells

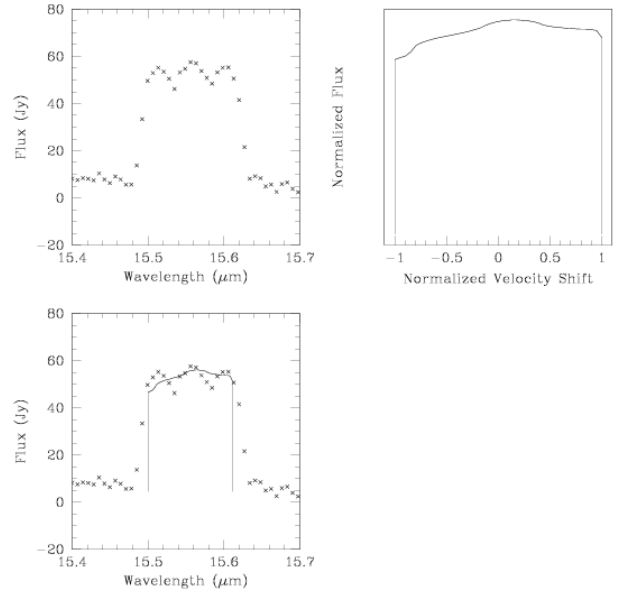


FIG. 7.— Top left: observed [Ne III] emission line from the WR colliding wind binary γ Vel. Top right: model line profile using the known parameters of the γ Vel system. Bottom left: an overplot of the data with our model for more direct comparison.

us that the companion is orbiting slower at apastron.

Figure 7 shows data taken by the Infrared Space Observatory of γ Velorum. Specifically, the data focuses on the [Ne III] line, which is at $15.56 \mu\text{m}$ (van der Hucht 1996). The parameters for this WR and O binary system have been determined through other methods. The model above plots the emission profile with the known parameters of $\beta = 85^\circ$, $i = 63^\circ$, $e = 0.326$, and $\omega = 68^\circ$ (Henley, Stevens, & Pittard 2005). Here, ω is the orbital phase angle between the line of sight and the major axis. Using these same parameters, our model is shown as a solid line plotted with the data as points. The model fails to reproduce the triple peak. It could

be that our model overlooks certain significant features, such as the emission from the compressed wind at the shock layer. Most likely, the shock layer contributes significantly to the total emission. Further efforts on this topic will need to include this important feature.

This project was funded by a partnership between the National Science Foundation (NSF AST-0552798), Research Experiences for Undergraduates (REU), and the Department of Defense (DoD) ASSURE (Awards to Stimulate and Support Undergraduate Research Experiences) programs.

REFERENCES

- Canto, J., Raga, A. C., & Wilkin, F. P., 1996, *ApJ*, 469, 729
Carroll, B., & Ostlie, D., 1996, *An Introduction to Modern Astrophysics*, Addison-Wesley Publishing Company, Inc.
Cassinelli, J., & Lamers, H., 1999, *Introduction to Stellar Winds*, Cambridge University Press, New York.
Henley, D., Stevens, I., & Pittard, J., 2005, *MNRAS*, 356, 1308
Ignace, R., & Brimeyer, A., 2006, *MNRAS*, 371, 343
Ignace, R., Cassinelli, J.P., Quigley, M., & Babler, B., 2001, *ApJ*, 558, 771
Lührs, S., 1997, *PASP*, 109, 504
Mihalas, D. 1978, *Stellar Atmospheres* (San Francisco: Freeman)
Van der Hucht, K.A., et al., 1996, *A&A*, 315, L193